CrossMark

Studies the effects of bath pH and lead molar concentrations on the structural, optical and electrical properties of lead sulphide thin films prepared by chemical route

Fekadu Gashaw Hone[1,2] · F. B. Dejene[1]

Abstract

Lead sulphide (PbS) nanocrystalline thin films were prepared by chemical bath deposition route from two different chemical baths. The first bath (bath-A) was synthesized by varying the volume of ammonia to study the effect of bath pH, while the second bath (bath-B) was complexed by potassium hydroxide and the effect of lead molar concentrations were investigated. The X-ray diffraction analyses confirmed that all deposited thin films from the two baths had face centered cubic crystal structure. The XRD results also verified that the crystalline size increased from 25 to 40 nm when lead molar concentration decreased to 0.1 M. The HRTEM images showed that the grains are grown along different planes which confirmed a typical polycrystalline nature of the deposited PbS thin films from both chemical baths. The elemental analyses were carried out by EDX and confirmed the formation of PbS compound. The optical absorption study showed that the lowest optical band gap of 0.81 eV was estimated from bath-B at 0.1 M lead concentration, whereas, a highest band gap of 1.57 eV was found from bath-A. The transmittance study verified that the transmittance was increased with the wavelength and the maximum transmittance was measured around 24.51% for pH 10.5. The photoluminescence study revealed that the PbS thin film exhibited a broadband emission spectra from 410 to 625 nm regardless of bath pH and lead concentration. The dc-two point probe measurement verified that the electrical properties of the PbS thin films were considerably changed by bath pH and lead molar concentrations. The room temperature resistivity of the thin films found in the order of 10^4 Ω cm.

1 Introduction

In recent years there has been an increasing interest in the synthesis of nanocrystalline materials due to their outstanding physical and chemical properties and their prospective applications [1]. Lead sulphide (PbS) nanocrystals among group IV–VI compound semiconductors has a face centered cubic crystal structure with space group $Fm\bar{3}m$ [2]. Since discovered early 19th, PbS attracted considerable attention due to its especially small direct band gap 0.41 eV and large exciton Bohr radius (~ 18 nm) [3]. PbS exhibits strong quantum size effects below excitonic Bohr radius and hence the energy band gap of its nanocrystals can be

tuned to anywhere between 0.41 and 5.2 eV [4]. Quantum-sized PbS can be useful in many applications, particularly in electroluminescent devices such as light emitting diodes and high speed switching and IR detectors. In solar energy research, PbS thin films have been investigated for photothermal conversion applications, either independently on metallic substrates or in multilayer stacks of PbS–CdS–PbS, $(PbS)_{1-x}(CdS)_x$ composites [5]. Lead sulphide has been also recommended as an earth abundant sustainable material for affordable photovoltaic devices [6].

A wide variety of deposition techniques are used so far for coating PbS thin films like Green hydrothermal [7], Successive ionic layer adsorption and reaction [8], Spray pyrolysis [9], Spin-coating [10] and chemical bath deposition (CBD) [11, 12]. Among aforementioned methods, CBD is one of important technique which attracting considerable attention due to its low temperature compatibility, large area deposition with better homogeneity. Moreover, it is relatively simple, cost effective with good reproducibility. The characteristics of chemically synthesized thin films strongly depend on the growth parameters like deposition

✉ Fekadu Gashaw Hone
  fekeye@gmail.com

1 Department of Physics (Qwa Qwa Campus), University of the Free State, Phuthaditjhaba, South Africa

2 Department of Physics, Hawassa University, P.O. Box: 05, Hawassa, Ethiopia

time, bath temperature, concentration of reactants, bath pH etc [13]. The optimization of these deposition parameters leads to nanoparticles with different size and shapes exhibiting different structural, optical and electrical properties [14]. The physical properties of thin films such as film thickness, crystalline size, optical band gap and surface roughness can be easily controlled by varying the growth parameters for different optoelectronic applications. Literature review showed that there are several works have been done to synthesize PbS thin films from low lead ion concentration (< 0.15 M) [11, 15, 16], however, only few reports are available on the deposition of PbS thin films from high lead molar concentrations [12, 17]. It was also observed that the effect of lead molar concentration and bath pH on the photoluminescence and electrical properties of PbS thin films are rarely reported. In the present work, the effect of lead molar concentration and bath pH on the structural, morphological, optical, photoluminescence and electrical properties of lead sulphide thin films were systematically investigating. Furthermore, effort had been made to optimize the deposition condition for relatively high lead molar concentrations by varying the bath pH.

2 Experimental details

2.1 Synthesis of PbS thin films

PbS thin films were deposited on silica glass substrate. The glass slides were degreased in nitric acid overnight then washed thoroughly with detergent and subsequently kept in ethanol about an hour, then after, ultrasonically cleaned with distilled water to remove any adhering impurities and dried under ambient conditions before being used for the deposition. In the present study, two baths with different chemical compositions were prepared to deposit PbS thin films in a 100 ml beaker. The first bath (bath-A) contained an aqueous solution of 5 ml (0.25 M) lead acetate trihydrate, 0.2 M thiourea, potassium hydroxide and ammonia (28%). Potassium hydroxide and ammonia was used as complexing agents and to get favorable pH. The PbS thin films deposited at three different pH (10.5, 11.5 and 12.0) by changing the volume of ammonia. The total volume of the chemical bath was maintained at 65 ml by adding enough amount of distilled water. The second bath (bath-B) was prepped by mixing 5 ml lead acetate trihydrate and 10 ml potassium hydroxide (0.2 M). Then about 5 ml ammonia (28%) added drop wise to use as a secondary complexing agent and to adjust the pH of the bath around 12 (optimal value obtained from bath-A). Thiourea (0.2 M) and some distilled water were added to obtain a final volume of 65 ml. Five different PbS thin films were synthesized by varying the concentration of lead acetate trihydrate from 0.1 to 0.3 M per step of 0.05 M. All the chemicals used

were Sigma-Aldrich product obtained from Lasec SA (Pty) Ltd, South Africa without further purification. The purity of the chemicals used was quoted by the manufacturers as 99.99%. In both deposition conditions the bath temperature was maintained at 70 °C. Chemically cleaned substrates were immersed vertically into the above prepared solutions and the reaction mixtures were maintained at a continuously magnetic stirring till the end of the deposition. Clear and colorless solution was observed at the beginning of the deposition for both baths then it changed to dark gray and later, a mirror-like film began to deposit onto the sides of the beaker and the substrate. After 30 min the samples were removed from the solution, rinsed ultrasonically with distilled water and dried under ambient conditions before film characterization. The as-deposited PbS thin films from the two baths were uniform, reflective and extremely adherent to the glass substrates.

2.2 Characterization

The crystallographic structure of PbS thin films were characterized by Bruker D8 advance diffractometer with CuK$_\alpha$ (1.5406 Å) radiation and the machine was operated at 40 mA and 40 kV. The elemental composition and surface morphology of the samples were studied using energy dispersive X-ray analysis (EDX) equipped with a high resolution JEOL JSM-7800F field-emission scanning electron microscope (FESEM). Carbon coating was used during EDX/SEM measurement to prevent charging. High resolution transmission electron microscopy (HRTEM) model TECNAI F3O S/ TEM used to investigate shapes and crystallographic nature of PbS thin films. The absorption spectrum was examined by Perkin Elmer Lambda 950 UV–Vis-NIR Spectrophotometer within the wavelength range of 250–2000 nm. Room temperature photoluminescence spectroscopy (PL) measurements were carried out by use F-7000 FL Spectrophotometer. The dc-two point probe method was applied to investigate the variations of resistivity with temperature.

3 Results and discussion

3.1 X-ray diffraction analyses

Figure 1 shows the XRD patterns of PbS thin films deposited from bath-A (Fig. 1a) and bath-B (Fig. 1b). The diffraction patterns were well matched with the standard JCPDS data file reference code: 005-0592 for face centered cubic crystal structure. No impurity peaks were observed. The XRD result (see Fig. 1a) revealed that the PbS thin film deposited at a pH of 10.50 had very weak diffraction peak along the (200) plane. As the bath pH increased the intensity along the (111) plane increased significantly, moreover, the number of diffraction
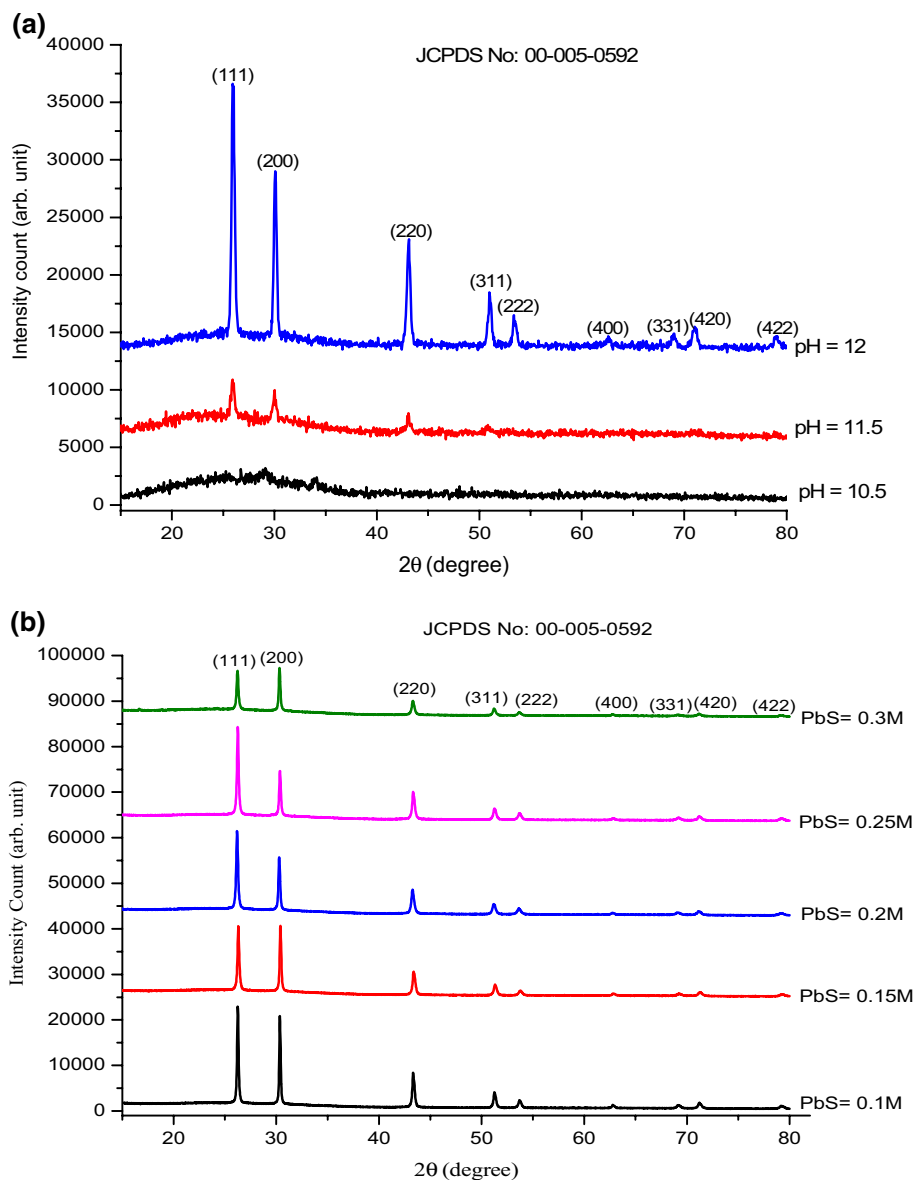
peaks were increased which indicating an improvement in the crystallinety nature of the prepared material [18]. Since thin film formation depends on the pH of the reaction mixture and pH depends on OH^- ions; the decrease in pH results in porous, non-reflecting and weakly adhered thin films on the substrates. At higher pH metal ion concentration will be lower and the reaction rate will be slow and resulting with well adherent and reflective thin film [19]. For the pH less than 10.5 it was noticed a non uniform and non adherent thin film which peeled off easily. The films deposited from bath-B (Fig. 1b) exhibited very sharp diffraction peaks corresponding to reflections from the (111), (200), (220), (311), (222), (400), (420) and (422) planes. This suggests that, PbS phase is stable and its formation is independent on the lead acetate concentration. But as the lead ion concentration increased from 0.1 to 0.3 M, the intensity of the diffraction peaks decreased. This may be

attributed due to the degradation of crystalline size because of a gradual precipitation of PbS due to excess Pb^{+2} ions in the chemical bath solution. Interestingly, noticed that varying pH and the lead molar concentration had a significant effect on the preferred orientations of the crystallites. The films deposited at lower pH $\approx$ 10.5, had a preferred orientation along the (200) plane but it was changed to the (100) plane when the chemical bath pH increased to 12. Similarly for the films deposited at 0.1, 0.2 and 0.25 M, the crystallites had a preferred orientation along the (111) plane, whilst for 0.15 and 0.3 M, the crystallites grown along the (200) plane. This indicates that the orientation of the grains growth along different directions depending on the lead molar concentration and bath pH. On the basis of the thermodynamics principle the basic reason for variation of preferred orientation is the change of the total system free energy during the film growth [20]. This behavior

of such preferred orientation changing was observed in many other works [11].

The average crystallite size (D) of PbS thin films were calculated from the FWHM found from X-ray diffraction pattern, using the Debye–Scherrer formula [11] which is given as:

$$D = \frac{K\lambda}{\beta_{2\theta}Cos\theta} \tag{1}$$

where, θ is the diffraction angle, β is the full width at half maximum of the most intense peak measured in radians, K is the constant known as the shape factor, taken as 0.94 and λ is the wave length of the X-ray radiation (1.5406 Å). The calculated crystallite sizes of PbS thin films deposited from bath-A and bath-B were in the range of 12–25 nm and 40–25 nm, respectively (see Table 1). The result suggested that the crystalline size increased while the bath pH increased. This may be ascribed the change of the involved chemical reactions in the bath to produce films with larger grain size at relatively higher bath pH. Similar observation was reported by [21]. In the contrary, the crystallite size calculated for the PbS thin films from bath-B was decreased as the molar concentrations of lead acetate increased (see Table 1). This inverse relationship between crystalline size and lead molar concentrations are rarely reported. This phenomena may explain interns of rapid precipitations of PbS. When the lead molar concentrations are increased in the chemical bath, rapid precipitation of PbS may occurred resulting only fewer ions available for film formation which leads the depositions of thinner films with smaller crystalline sizes. The average thickness of the thin films deposited from bath-A and bath-B were measured by weight difference method and found in the range of 125–342 nm and 285–627 nm respectively. It was noticed that as bath pH > 12.5 and the concentration of lead acetate increased further (> 0.3 M), a lot of dark precipitation, non uniform and very thin film was found. Lattice constant (a_{hkl}) for the cubic structure was calculated using Eq. (2) and the results are presented in Table 1.

$$a_{hkl} = d_{hkl}\overline{)h^2 + k^2 + l^2} \tag{2}$$

The calculated value of the lattice constant 'a_{hkl}' of the films shows a slight deviation from its standard value of 5.936 Å (see Table 1). The deviation of the calculated lattice constant from the bulk sample value indicates the crystallites may be under some strain [22]. The origin of microstrain may be due to the lattice mismatch between deposited material and substrate or depends upon the growing conditions of the thin films [23]. The microstrain value (ε) of the as-deposited PbS thin films were calculated from the mathematical relation in ref [13]. The other structural parameter calculated was the dislocation density (δ) which is a measure of the defects in the film [22], and this was calculated using Williamson and Smallman's formula [24]. Strain and dislocation density of the thin films were calculated from the (200) plane for bath-A and the (111) plane for bath-B and the results are tabulated in Table 1.

The values of strain calculated in this study is in good agreement with previously reported works [12]. Relatively large dislocation density was observed at bath pH 10.5, this showed that the film has comparatively lesser degree of crystallinity [22]. It was observed that the strain and dislocation density were decreased with increasing crystallite size for both baths (see Table 1). This may be due to a decrease in the occurrence of grain boundaries because of an increase in the crystallite size. Since dislocation density and strain are the manifestation of dislocation network in the thin films, the decrease in dislocation density with crystallite size indicates the formation of high quality thin films [25].

3.2 Elemental analyses

Figure 2 shows the representative EDX patterns of PbS thin films synthesized from bath-A and bath-B. The weight percentage found from the EDX analyses were converted in to atomic percentage (at.%). The EDX spectra of the PbS thin film deposited at a pH of 10.5 (Fig. 2a) displayed several peaks at different energy values, which are corresponds to Pb, S and other elements but the strong peak is from silicon. This is may be due to the formation of very thin film at this pH deposition. However, for the higher pH around 12 the EDX pattern of PbS thin film showed strong peaks from Pb and S elements (see Fig. 2c) and the average atomic percentage improved considerably (see Table 2). It is good to mansion here that, the EDX results verified that varying the chemical bath pH had a vital role on stoichiometric ratio of chemically deposited PbS thin films (see Table 2). This

Table 1 Crystallographic parameters of PbS thin films deposited from bath-A and bath-B

	Bath-A			Bath-B				
Deps. conditions	pH 10.5	pH 11.5	pH 12	0.1 M	0.15 M	0.2 M	0.25 M	0.3 M
Crystallite size (nm)	12.52	18.02	29.24	40.66	38.13	34.72	29.24	25.63
Lattice constant (nm)	5.951	5.942	5.933	5.934	5.936	5.938	5.933	5.932
Strain (ε) ($\times 10^{-3}$) lines^{-2} m^{-4}	25.847	14.302	3.285	1.018	2.545	3.508	3.285	8.870
Dislocation density ($\times 10^{-3}$) lines/m^2	63.796	30.795	11.696	6.049	6.878	8.295	11.696	15.223
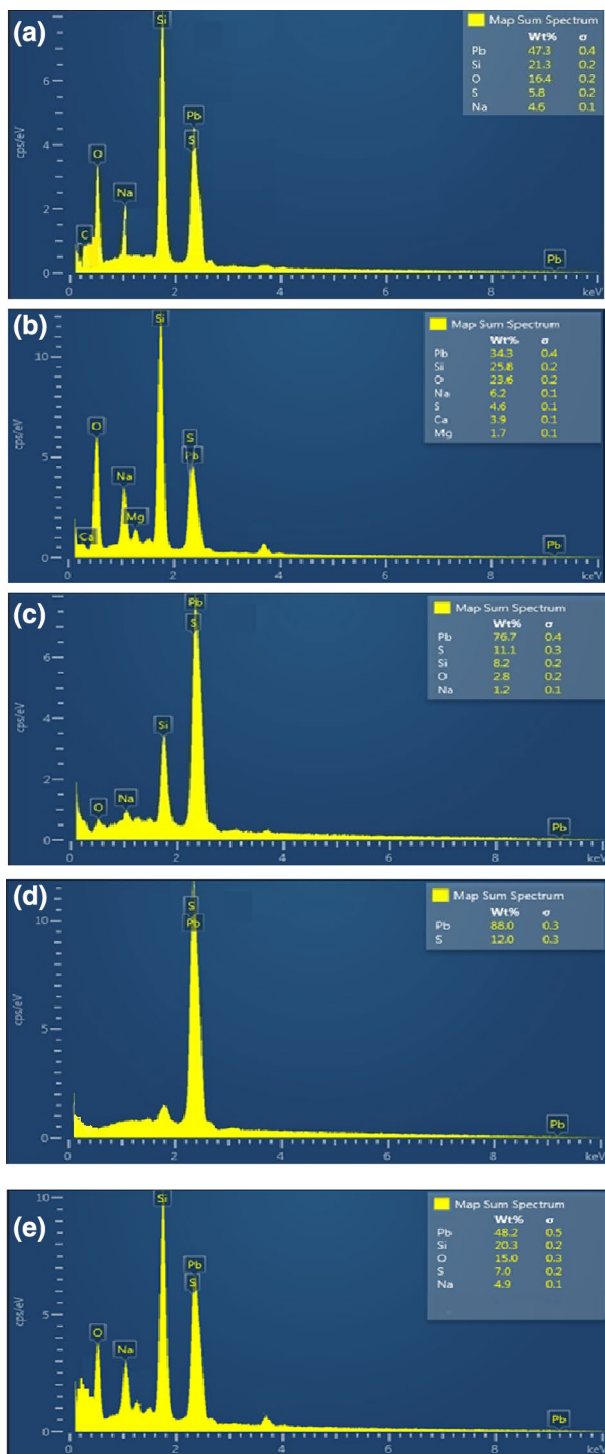
Fig. 2 EDX spectra of PbS thin films: **a** at pH 10.5 **b** at pH 11.5 **c** at pH 12 (bath-A and bath-B) **d** Pb^{+2} = 0.1 M and **e** Pb^{+2} = 0.3 M

variation of stoichiometric ratio of chemically deposited PbS thin films with pH may be due to the growth mode of the thin film which facilitates the reaction solution to uphold better stoichiometry ratio at higher bath pH. The EDX results also confirmed that there was no significant stoichiometric

ratio variation was observed as the lead acetate concentration changed from 0.1 to 0.3 M. The EDX study further established that irrespective of the deposition conditions all the deposited PbS thin films were lead reach. As a consequence, some defects like S vacancies or Pb interstitial will be inhibited at a certain level, which will facilitate the application of PbS thin film in photovoltaic devices. Since silica glass substrates were used for film deposition; Si, Mg, Ca and Na peaks were observed in EDX analysis (see Fig. 2a, b). The intensity of the observed spectrum from the above mentioned elements decreased or disappeared when the stoichiometric ratio increased (see Fig. 2c). This may be due to thicker film deposited for higher pH, leading to reduce the signals emanating from the substrate. The oxygen content found in the EDX spectrum could either from the substrate or due to the films getting oxidized on exposure to the atmosphere [18]. The carbon peak was due to the carbon tape used during EDX analyses.

3.3 Scanning electron microscopy (SEM) studies

The FESEM images of chemically deposited PbS thin films from bath-A and bath-B are displayed in Fig. 3. The SEM micrograph of PbS thin film deposited at a pH of 10.5 (Fig. 3a) shows very small spherically shaped grains with different sizes. Moreover, large isolated clusters of spherically shaped grains were observed on some parts of the micrographs indicating irregular growth rate of the grains. The formation of such aggregate grains on the PbS thin film surface is a typical future of the CBD technique. As the chemical bath pH increased (see Fig. 3b, c), the surface morphology of the PbS thin film becomes more homogeneous and covered the substrate very well. Also, the grain sizes were noticed to increase gradually, which is consistent with the XRD results. It was also verified that the shape of the grains changed from spherical to a mixture of cubic and pyramidal shape as the bath pH was changed from 10.5 to 12.0. The different growth rates on the (200) and (111) plans may responsible for formation of the spherical and pyramidal PbS crystals. Similar observation was reported by Tohidi et al. [26].

The SEM morphology of PbS thin films deposited from bath-B (see Fig. 3d), exhibited densely compact and sharp edges of the grains cover the entire surface without any visible defects like cracks or pinholes. It was noted that the grains have a mixture of rectangular and pyramidal like shape with different sizes. Increase in grain size favors coalescence between each grains during lateral growth which in turn explains increase in compactness of the deposited thin films [27]. From Fig. 3e, f it is clearly observed that as the lead molar concentration increased the grains loss their sharp edged nature and becomes smaller in size. The estimated average grain sizes of the

Table 2 EDX and optical band gaps of PbS thin films deposited from bath-A and bath-B

	Bath-A			Bath-B				
Deps. conditions	pH 10.5	pH 11.5	pH 12	0.1 M	0.15 M	0.2 M	0.25 M	0.3 M
Pb (at.%)	55.79	53.51	52.72	53.16	52.03	53.16	52.72	51.68
S (at.%)	44.21	46.49	47.28	46.84	47.97	46.84	47.28	48.32
Eg (eV)	1.57	1.42	1.05	0.81	0.97	1.01	1.05	1.15
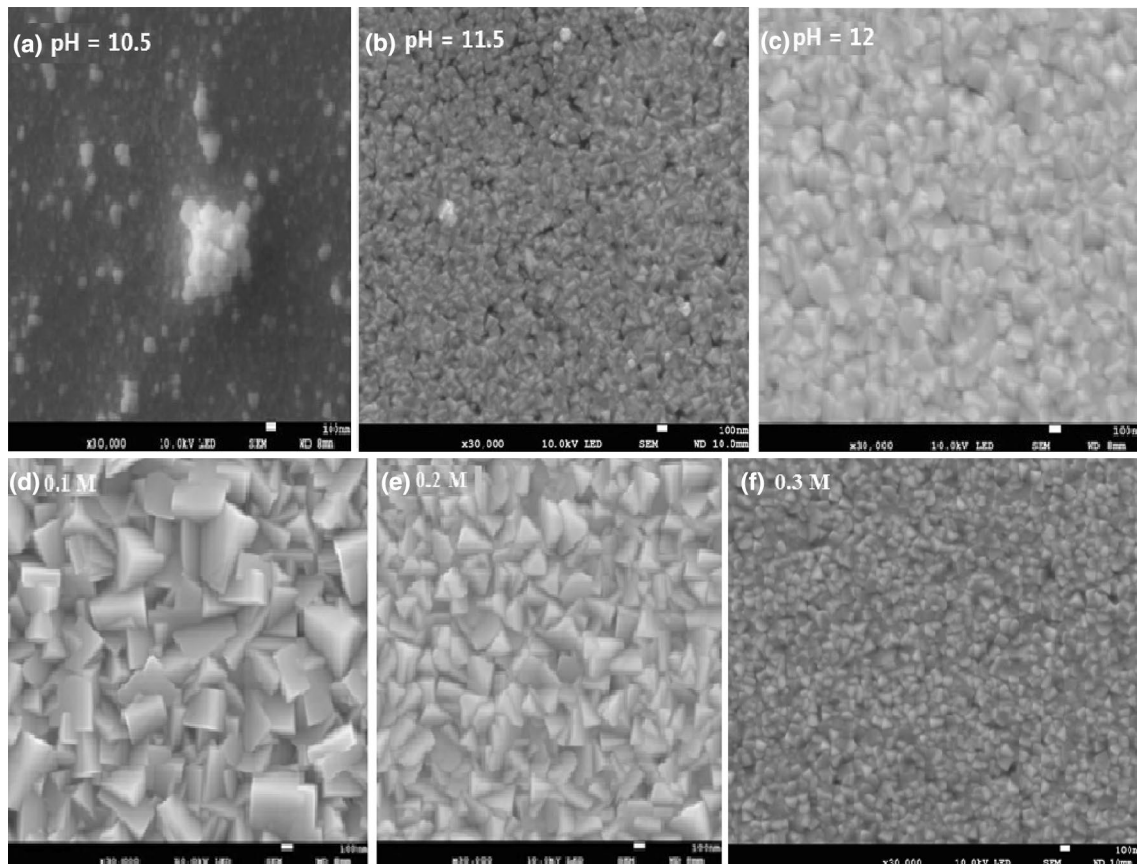
**Fig. 3** FESEM images of PbS thin films deposited from bath-A and bath-B

thin films from SEM images were in the range of 32–54 and 52–84 nm for bath-A and B respectively. The grain sizes calculated from SEM images are greater than those obtained using the Scherrer formula. This can be attributed to lager clusters deposited on the surface of the film, clearly show an aggregate structure composed of small crystals or grains and SEM images show these clusters on the surface of the thin film [28]. In fact, it is anticipated in the case of nanocrystalline thin films that the domains have a tendency to increase its size near the film surface, thus SEM images representing the surface features of the film, give maximum possible size of grains [29]. On the other hand, crystallite sizes calculated using the XRD data is thickness averaged magnitude, which usually dominated

by the smallest crystallites [28, 30]. Such grain size discrepancy between XRD and SEM were reported by several researchers [31].

3.4 High resolution transmission electron microscope (HRTEM) studies

Figure 4 shows a high resolution plane view of representative TEM micrographs and interplanar distances of the PbS thin films.

The TEM micrographs clearly shows that the nanocrystals are well dispersed with minimal aggregation. Figure 4a revealed that PbS thin film deposited from 0.1 M lead ion concentration is a mixture of cubic and rectangular crystals
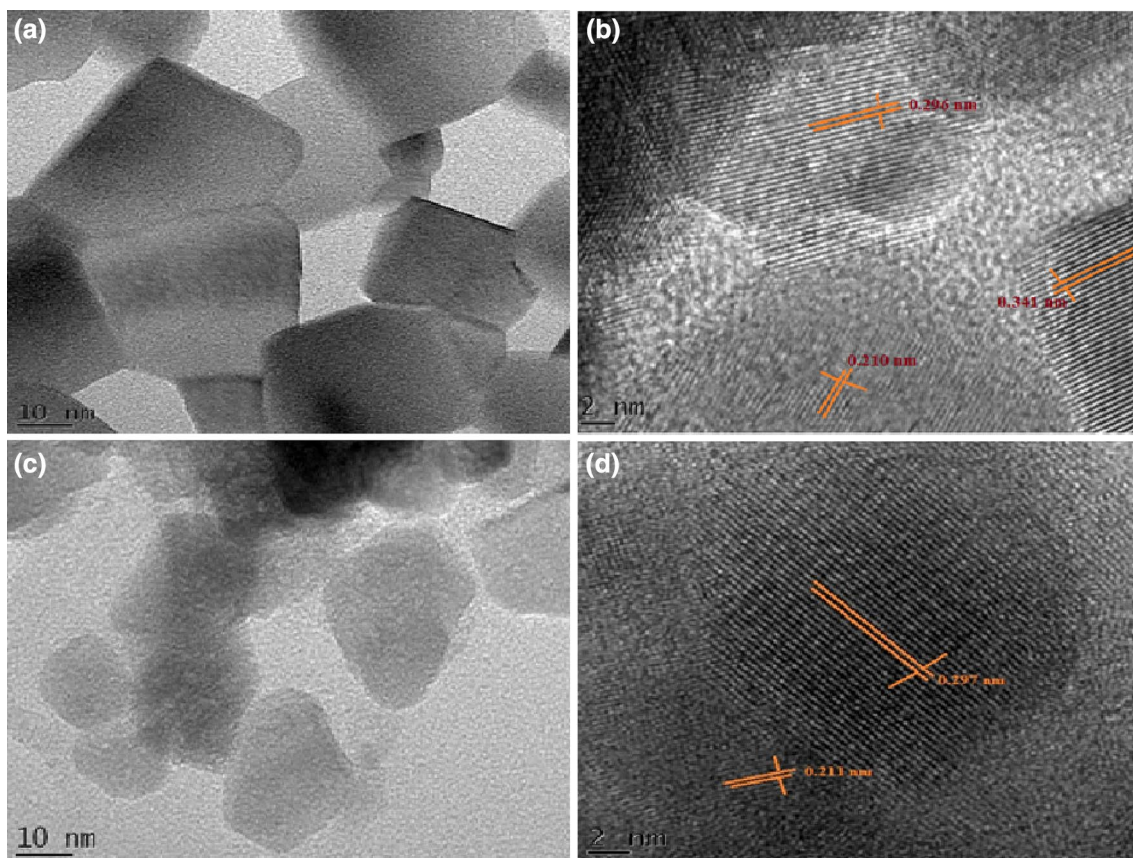
Fig. 4 TEM images of PbS thin films: **a** Pb^{2+} = 0.1 M and **c** Pb^{2+} = 0.25 M (pH 12). Interplanar distances of PbS thin films: **b** Pb^{2+} = 0.1 M and **d** Pb^{2+} = 0.25 M (pH 12)

with different size and orientations. It was also observed from Fig. 4a that the crystals are sharp edged and interconnected each others. This is consistent with SEM morphology. Figure 4c shows that nanocrystalline with different shape and sizes are attached together with a common crystallographic orientation. The lattice fringes shown in HRTEM images (Fig. 4b, d) confirm the perfect order of the crystalline lattice of the PbS thin films. The d-spacing of 0.341, 0.296 and 0.210 nm corresponds to the (111), (200) and (220) planes of the face centre cubic crystal structure of PbS respectively (see Fig. 4b). Similarly the d-spacing of 0.297 and 0.211 nm corresponds to the (200) and (220) planes of the fcc PbS respectively (see Fig. 4d). In general Fig. 4b, d plainly shows that the grains are grown along different planes which confirm a typical polycrystalline nature of the deposited PbS thin films from both baths. This observation is consistent with the XRD results.

3.5 Optical studies

3.5.1 Optical band gap determination

The optical band gap and transition type of nanocrystalline PbS thin films synthesized from the two baths were determined from the Stern relationship of near-edge absorption which is given as [13].

$$(Ahv)^2 = \left[k(hv - E_g)\right]^n \tag{3}$$

where v is the frequency, h is the Planck's constant, k is a constant while n carries either 1 or 4 depending on the optical transition. Since PbS is a direct band gap material [9], n was taken as 1. Figure 5 presents the Stern plot of $(Ahv)^2$ versus (hv) for the PbS thin films synthesized from bath-A and bath-B. The band gap values of the films were estimated
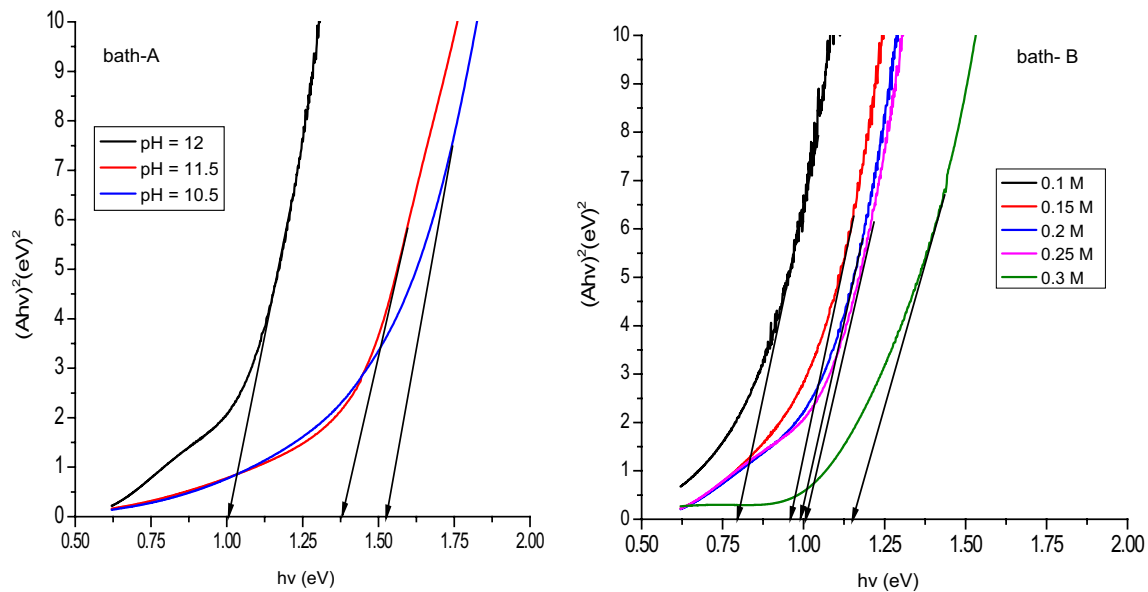
Fig. 5 The graphs of $(Ah\nu)^2$ plotted as a function of the photon energy for PbS thin films deposited from bath-A and bath-B

by extrapolating linear portion of the plots to the energy axis zero. The plot of $(Ah\nu)^2$ versus $(h\nu)$ shown in Fig. 5 is linear at the absorption edge which indicates the presence of direct transition. The optical band gaps of the PbS thin films obtained from bath-A and bath-B were estimated in the range of 1.05–1.57 and 0.81–1.15 eV respectively. The results verified that the optical band gap was decreased when the bath pH was increased, but a direct relationshipe was observed in the second chemical bath. The observed variation of optical band gap may be attributed to the variation of the average crystallite size, dislocation density and microstrain of the material with bath pH and lead molar concentration in the respective baths [18].

The optical band gap values of all the PbS thin films found from the two chemical baths are listed in Table 2. In this study the estimated band gap for PbS thin films from both baths shows a significant blue shift from the bulk value of 0.41 eV. For the thin films deposited from pH 10.5 and 11.5, this appreciable band gap shift may be due to quantum size effect exhibited by the nanocrystals present in PbS film [31]. But for the rest of the thin films, the quantum confinement effect may not be significant since the crystallite size is greater than 18 nm. The band gap tunability of the films having larger crystallite sizes beyond the quantum confinement regime may have different mechanisms [32]. For instant defects like vacancies, interstitials, grain boundaries, stacking faults, etc. can act as trap centers and affect the optical absorption. Therefore, an increase in optical band gap can be associated with defect-induced band tailing due to the creation of localized energy states near the band gap [33]. There are several

reports demonstrating variable band gaps of 0.8–2.3 eV in the case of PbS thin films for crystallites size with the range of 12–52 nm [28, 32, 34]. It is interesting to note that the deposition condition in bath-A gives PbS thin films with optical band gaps in the optimum range of solar cell absorber which capable of harnessing photons over the visible regime. This would help to prepare an efficient solar absorber to absorb the maximum span of the solar spectrum in PbS based solar cells. The transmittance of all prepared thin films were carried out with a UV–Vis-NIR spectrophotometer at room temperature and the spectra is displayed in Fig. 6.

From the transmittance curves it is clearly observed that the transmittance is increased with the wavelength and the maximum transmittance was measured 24.51 and 23.52% for pH 10.5 and 0.3 M lead molar concentration respectively. It was also noticed that the transmittance decreased while the bath pH increased from 10.5 to 12 and the lead concentration decreased from 0.3 to 0.1 M. This may be attributed to the formation of thick, uniform and highly crystalline nature of thin films. Similar observation was reported in Refs. [11, 35]. From the figures it was also observed that the transmittance of all PbS thin films were very low in the visible region. In this region the incoming photons have sufficient energy to excite electrons from the valence band to the conduction band which leads these photons are absorbed within the material to decrease the transmittance [22]. Relatively high transmittance in the NIR region was observed for PbS thin films deposited from pH 10.5 and 0.3 M lead concentration. This nature will make them a good candidate for antireflection coating and house heating for solar chick brooding.
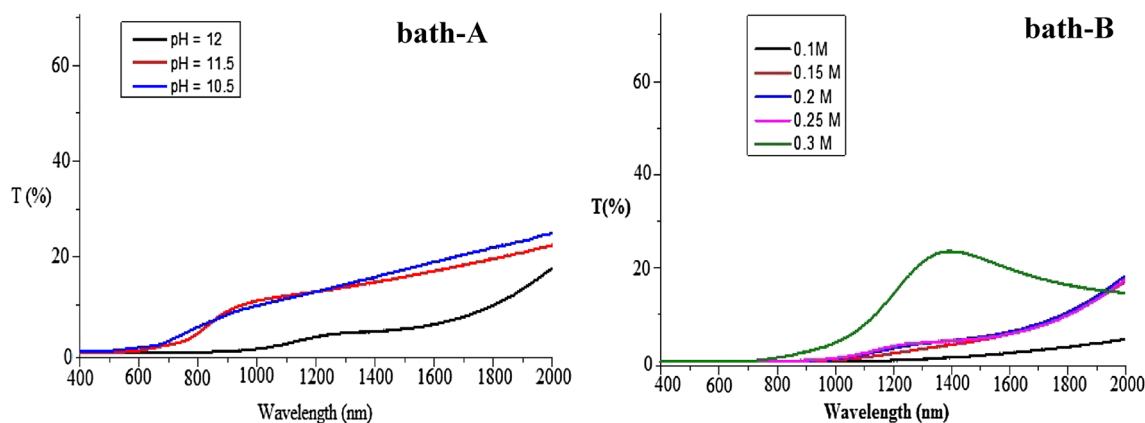
Fig. 6 Transmittance versus wavelength curves for PbS thin films deposited from bath-A and bath-B

3.5.2 Photoluminescence studies

Photoluminescence (PL) is a process in which an electron excited by a monochromatic photon beam of certain energy under goes nonradiative/radiative recombination either at valance band or at traps/surface states. The band edge luminescences in general are weak whereas efficient luminescence transfer occurs at traps/surface states [4]. The photoluminescence emission spectra of PbS thin films deposited from the two baths are displayed in Fig. 7. The measurement was made at an excitation wavelength of 308 nm using a Xenon lamp at room temperature. Regardless of bath pH and lead molar concentrations, the PL spectra showed broadband emission in the range of 410–625 nm. It was also observed well defined twin peaks around 451 and 465 nm with a shoulder at 526 nm. Such broadband PL emissions from UV to infrared regions have been reported in previous works, which suggest more comprehensive investigation still needed for PL properties of PbS compound. Kaci et al. [36]

observed an intense and broadband emission for PbS thin film at excitation of 230 nm. The broad emission peaks were at 367, 386, 411, 448, 475 and 533 nm. Tohidi et al. [26] also reported a broadband emission for PbS thin film prepared at differ deposition time and they found two emission peaks at 351 and 451 nm with an excitation of 320 nm. Ye et al. [37] prepared self-assembly one-dimensional PbS nanocrystals and reported two peaks at 332 and 373 nm. Pawar et al. [38] also reported emission peaks at 393, 405 and 460 nm with excitation wavelength of 416 nm for PbS samples.

Bulk PbS semiconductor is narrow direct band gap of 0.41 eV at room temperature which gives rise emission about 3024 nm. But in this study all the PL spectra showed a blue-shift similar to the absorption results. The shifting of the emission wavelengths from 3024 to 451 nm for the two baths can be ascribed to a high level transition in PbS semiconductor crystallites [7]. It has been also reported that this kind of band edge luminescence arises from the recombination of excitons and/or sub-band gap surface states [39].
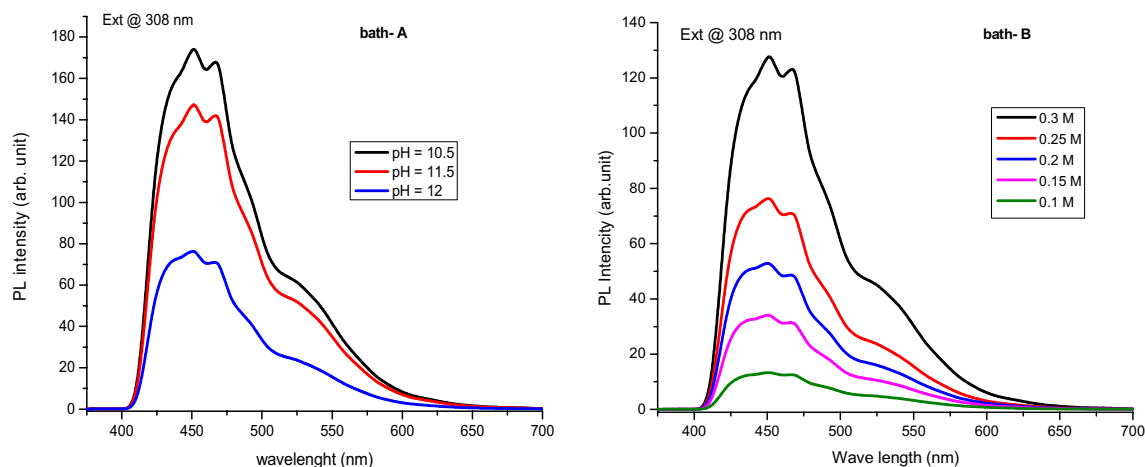
Fig. 7 Room temperature photoluminescence emission spectra of PbS thin films prepared from bath-A and bath-B

The peaks at 465 nm may be attributed to the transitions of trapped electrons to the valence band from donor levels [40]. From Fig. 7b, it is noticed that as the lead molar concentration increased the peak around 465 nm gradually decreased and disappeared at 0.1 M. It is worth enough to highlight here that, in comparison with colloidal quantum dots, CBD films are generally not deliberately passivated and both the intensity and spectral shape can vary considerably without any obvious reason [26]. In semiconductor nanoparticles excitonic and surface state luminescence emissions are generally observed, but the luminescence of semiconductor nanocrystals generally arises from the surface states (dangling bonds, defect sites and traps). The excitonic emission is sharp and is located near the absorption edge of the particles, while the surface-state emission is broad and shows a Stokes' shift which indicates trapped luminescence arising from the surface states in the PbS nanoparticles [41]. The broad emission in the present study may be attributed with this phenomenon. Several research results verified that the luminescence intensity depends on the surface area of the grains. The materials with smaller crystallites size showed higher luminescence intensity compared to the larger crystallites [42]. Similar trained was observed in the present study (see Fig. 8). In thin film, the number of ions on the surface quickly increases as the crystalline size decreases (higher surface-to-volume ratio). Furthermore, carrier recombination rate increases as size decreases because of the increase in overlap between the electron and hole wave functions. These two effects may cause PL intensity to increase as particle size decreases [43]. Hence, PbS thin film synthesized from bath pH 10.5 improve the emission intensity and broadens of the emission range. This feature is extremely useful to enhance the performance of different photonic devices such as light emitting diodes, lasers, as well as luminescence based sensors [26]. In the present study the PL result verified that the PL emission spectra position of the peaks remain the same for all PbS thin films which infer that they exhibit the same crystal structure irrespective of lead ions concentration and bath pH which is consistent with XRD results.

3.6 Electrical property studies

In the present study, dc-two point probe method was applied to investigate the effects of bath pH and lead molar concentrations on the electrical resistivity (ρ) and conductivity (σ) of PbS thin films. The resistivity investigation was carried out in the temperature range of 300–400 K using silver contacts. The variations of ln ρ with reciprocal of temperature, $(1/T) \times 10^3$ plotted and illustrated in Fig. 9. From the figure it is seen that resistivity decreases with temperature, indicating semiconducting nature of the thin films. It is also observed that, the nature of all thin films deposited from the two baths are very similarly over the studied range with temperatures. This shows that the same conduction mechanisms are dominant for all compositions [44].

The estimated room temperature resistivity and conductivity values of PbS thin films prepared from the two different chemical baths are summarized in Table 3.

From Table 3 it is clearly observed that the electrical properties of the PbS thin films significantly affected by bath pH and lead molar concentrations. The highest resistivity in the order of 10^4 Ω cm was measured for PbS thin film deposited from bath-A at a pH of 10.5. This is may be due to its poor crystallinity which indicates the presence of few atomic layers of disordered atoms [45]. The observed high resistivity decreased in the order of 10^2 Ω cm as the bath pH increased to 12. Relatively the smallest resistivity of 77.6 Ω cm and highest conductivity of 128.465×10^{-4} $(\Omega \text{ cm})^{-1}$ were recorded from bath-B at 0.1 M lead concentration. The decrease in resistivity of the thin films observed in the present study may attributed to enhancement of carrier concentration due to an improvement of crystallinity which

Fig. 8 PL intensity versus crystalline size for PbS thin films deposited from bath-A and bath-B
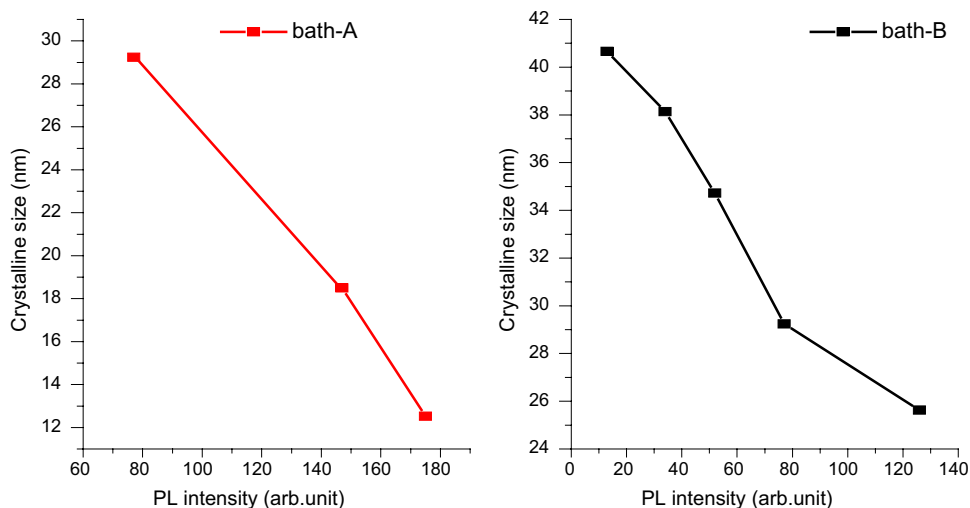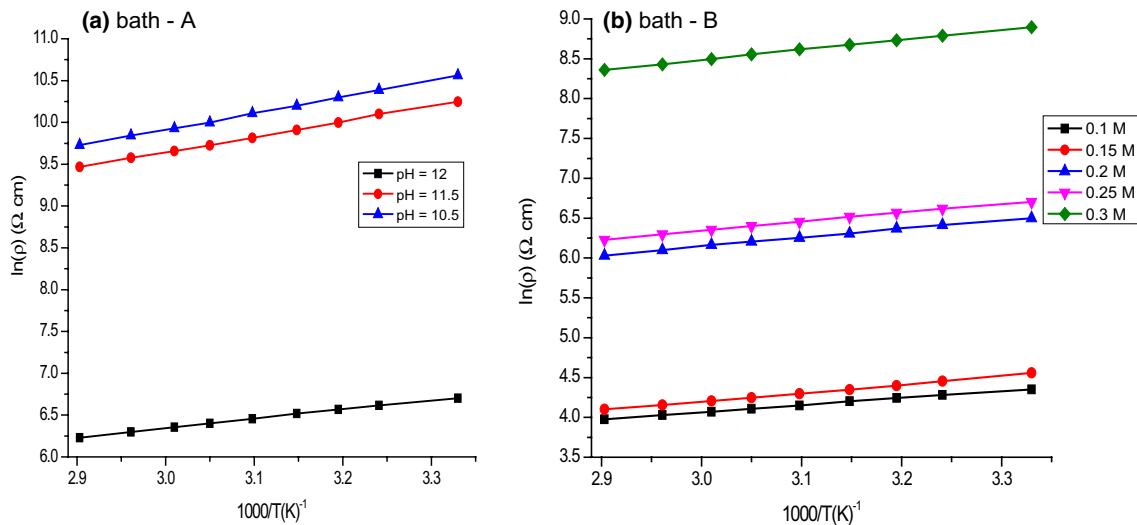
Fig. 9 Variations of ln ρ versus 1000/T for PbS thin films deposited from bath-A and bath-B

Table 3 Optical band gap and electrical parameters of PbS thin films deposited from the two baths

	Bath-A			Bath-B				
Deposition conditions	pH 10.5	pH 11.5	pH 12	0.1 M	0.15 M	0.2 M	0.25 M	0.3 M
Eg (eV)	1.57	1.42	1.05	0.81	0.97	1.01	1.05	1.15
RT $\rho \times 10^4$ (Ω cm)	3.860	2.819	0.0815	0.00776	0.00954	0.0663	0.0815	0.7295
RT $\sigma \times 10^{-4}$ (Ω cm)$^{-1}$	0.386	0.354	12.269	128.465	104.823	15.083	12.269	1.371
ε (eV)	1.955	1.837	1.121	0.893	1.066	1.102	1.121	1.258

Eg Optical band gap, *RT* Room temperature, *ε* Activation energy

leads to reduction of grain boundary scattering. These phenomena may increase the acceptor states and hole carrier concentration in the valence band and leads to low resistivity at room temperature [46]. The presence of defects such as structural disorders, dislocations and surface imperfections also play an important role in decreasing the conductivity as reported in several previous works [44, 47]. The temperature dependence of electrical resistivity (ρ) of the thin films follows the Arrhenius law and is given by

$$\rho = \rho_0 \, e^{(E_0/KT)} \tag{4}$$

where, ρ is resistivity at temperature *T*, ρ_0 is a constant, T is absolute temperature, *K* is Boltzmann constant (8.62×10^{-5} eV/K) and E_0 is the activation energy required for conduction. The thermal activation energy estimated from Eq. 4 for all prepared PbS thin films are listed in Table 3. The activation energy found in the range of 1.955–1.121 and 0.893–1.258 eV for PbS thin films prepared from bath-A and bath-B respectively. From Table 3 it was observed that the activation energy reduced with increasing of bath pH and decreases of lead molar concentration, this may be due to an improvement of the electrical conductivity

of the deposited PbS thin films. The decrease in activation energy also reflects in the decrease in the band gap of the thin films which is consistent with the results found from optical band gap measurements however there is a variation in the estimated values. The above results confirmed that bath pH and lead molar concentration plays a vital role in the electrical properties of PbS thin films.

4 Conclusion

Lead sulphide thin films were successfully synthesized via chemical bath deposition method from two different chemical baths at a bath temperature of 70 °C. The effect of the lead molar concentration and bath pH on the structural, morphological, optical and electrical properties has been well established. The XRD results confirmed that varying the bath pH and lead molar concentrations had a significant effect on the preferred orientations and microstructure parameters of the deposited thin films. The EDX results verified that varying the bath pH had a vital role on the stoichiometric ratio of PbS thin films but there was no significant stoichiometric ratio variation was observed as the lead

molar concentration changed. The TEM morphology studies confirmed that PbS thin films deposited from both baths are composed of rectangular and irregular shaped crystals with different sizes and orientations. The optical band gap of the PbS thin films obtained from bath-A and bath-B were estimated in the range of 1.05–1.57 and 0.81–1.15 eV respectively. Relatively a maximum transmittance spectrum was observed for PbS thin film prepared from 0.1 M lead molar concentration. The PL study revealed that the PbS thin film exhibited a broadband emission spectra from 410 to 625 nm. The PL emission spectra also confirmed that the maximum emission peak was observed for PbS thin film deposited from bath-A at a pH of 10.5. The room temperature resistivity of the thin films found in the order of 10^4 Ω cm and decreased as the bath pH increased. The electrical property study revealed that the thermal activation energy had direct relationship with lead molar concentration and found in the range of 1.258–0.893 eV.

References

1. A.-C. Reádigos, V.M. García, O. Gomezdaza, J. Campos, M.T.S. Nair, P.K. Nair, Semicond. Sci. Technol. **15**, 1022 (2000)
2. S.I. Sadovnikov, A.I. Gusev, J. Alloy. Compd. **573**, 65 (2013)
3. F.D. Martinez-Mancera, J.L. Hernandez-Lopez, Mater. Chem. Phys. **148**, 1045 (2014)
4. S.N. Sahu, K.K. Nanda, PINSA **67**, 103 (2001)
5. L.P. Deshmukh, B.M. More, S.G. Holikatti, P.P. Hankare, Bull. Mater. Sci. **17**, 455 (1994)
6. W. Cyrus, A.P. Alivisatos, D.M. Kammen, Environ. Sci. Technol. **43**, 2072 (2009)
7. M. Mohammadikish, F. Davar, J. Mater. Sci.: Mater. Electron. **26**, 2937 (2015)
8. E. Yücel, Y. Yücel, B. Beleli, J. Cryst. Growth **422**, 1 (2015)
9. S. RaviShankar, A.R. Balub, M. Anbarasi, V.S. Nagarethinam, Optik **126**, 2550 (2015)
10. J. Patel, F. Mighri, A. Ajji, D. Tiwari, T. Chaudhuri, Appl. Phys. A Mater. Sci. Process. **117**, 1791 (2014)
11. S. Seghaier, N. Kamoun, R. Brini, A.B. Amarac, Mater. Chem. Phys. **97**, 71 (2006)
12. N. Choudhury, B.K. Sarma, Thin Solid Films **519**, 2132 (2011)
13. F.G. Hone, F.K. Ampong, T. Abza, I. Nkrumah, M. Paal, R.K. Nkum, F. Boakye, Mater. Lett. **155** 58 (2015)
14. F. Göde, E. Güneri, F.M. Emen, V. Emir Kafadar, S. Ünlü, J. Lumin. **147**, 41 (2014)
15. L. Rajen Singh, S. Bobby Singh, R.K. London, H.B. Sharma, A. Rahman, AIP Conf. Proc. **146**, 353 (2012)
16. A. Hussain, A. Begum, A. Rahman, Indian J. Phys. **86**, 697 (2012)
17. N. Choudhury, B.K. Sarma, Bull. Mater. Sci. **32**, 43 (2009)
18. F.G. Hone, F.K. Ampong, Mater. Chem. Phys. **183**, 320 (2016)
19. P.P. Hankarea, S.D. Delekara, M.R. Asabea, P.A. Chatea, V.M. Bhusea, A.S. Khomanea, K.M. Garadkarb, B.D. Sarwade, J. Phys. Chem. Solids **67**, 2506 (2006)
20. S. Xigui, K. Gao, X. Pang, H. Yang, ACS Appl. Mater. Interfaces **8**, 625–633 (2016)
21. K.C. Preetha, K.V. Murali, A.J. Ragina, K. Deepa, T.L. Remadevi, Curr. Appl. Phys. **12**, 53 (2012)
22. B. Rajashree, A.R. Balu, V.S. Nagarethinam, Int. J. Chem. Tech. Res. **6**, 347 (2014)
23. A.N. Chattarki, S.S. Kamble, L.P. Deshmukh, Mater. Lett. **67**, 39 (2012)
24. G.K. Williamson, R.E. Smallman, Phil. Mag. **1**, 34 (1956)
25. M.R.A. Bhuiyan, M.A.A. Azad, S.M.F. Hasan, Indian J. Pure Appl. Phys. **49**, 180 (2011)
26. T. Tohidi, K. Jamshidi-Ghaleh, Appl. Phys. A **118**, 1247 (2015)
27. M.P. Deshpande, N. Garg, S.V. Bhatt, P. Sakariya, S.H. Chaki, Mater. Sci. Semicond. Process. **16**, 915 (2013)
28. H. Sattarian, T. Tohidi, S. Rahmatallahpur, Mater. Sci. **34**, 540 (2016)
29. G. Korotcenkov, A. Cornet, E. Rossinyol, J. Arbiol, V. Brinzari, Y. Blinov, Thin Solid Films **471**, 310 (2005)
30. S. Thangavel, S. Ganesan, S. Chandramohan, P. Sudhagar, Y.S. Kang, C.H. Hong, J. Alloy. Compd. **495**, 234 (2010)
31. N.B. Kotadiya, A.J. Kothari, D. Tiwari, T.K. Chaudhuri, Appl. Phys. A **108**, 819 (2012)
32. D.H. Yeon, S.M. Lee, Y.H. Jo, J. Moon, Y.S. Cho, J. Mater. Chem. A **2**, 20112 (2014)
33. O.P. Moreno, R.G. Pérez, R.P. Merino, M.C. Portillo, G.H. Téllez, E.R. Rosas, Thin Solid Films **616**, 800 (2016)
34. D. Kumar, G. Agarwal, B. Tripathi, D. Vyas, V. Kulshresth, J. Alloy. Compd. **484**, 463 (2009)
35. M.M. Abbas, A.A. Shehab, N.A. Hassan, A.K. Al-Samuraee, Thin Solid Films **519**, 4917 (2011)
36. S. Kaci, A. Keffous, L. Guerbous, M. Trari, Thin Solid Films **520**, 79 (2011)
37. S. Ye, Y. Ye, Y. Ni, Z. Wu, J. Cryst. Growth **284**, 172 (2005)
38. S.B. Pawar, J.S. Shaikh, R.S. Devan, Y.R. Ma, D. Haranath, P.N. Bhosale, P.S. Patil, Appl. Surf. Sci. **258**, 1869 (2011)
39. S. Kaci, A. Keffous, M. Trari, O. Fellahi, A. Menari, A. Manseri, L. Guerbous, J. Lumin. **130**, 1849 (2010)
40. C. Rajashree, A.R. Balu, V.S. Nagarethinam, J. Mater. Sci.: Mater. Electron. **27**, 5070 (2016)
41. T. Tohidi, K. Jamshidi-Ghaleh, Phil. Mag. **94**, 3368 (2014)
42. N. Akin, Y. Ozen, H.I. Efkere, M. Cakmaka, S. Ozcelik, Surf. Interface Anal. **47**, 93 (2014)
43. X. Wang, F. Zhao, P. Xie, S. Deng, N. Xu, H. Wang, Chem. Phys. Lett. **423**, 361 (2006)
44. S. Hassanien, A.A. Akl, Superlattices Microstruct. **89**, 153 (2016)
45. J.Y.W. Seto, J. Appl. Phys. **46**, 5247 (1976)
46. K.S. Kumar, A.G. Manohari, C. Lou, T. Mahalingam, S. Dhanapandian, Vacuum **128**, 226 (2016)
47. F.G. Hone, F.B. Dejene, Mater. Res. Express **5**, 026409 (2018)